# Symmetry breaking of solitons in two-component Gross-Pitaevskii equations

Hidetsugu Sakaguchi[1] and Boris A. Malomed[2]
[1]*Department of Applied Science for Electronics and Materials, Interdisciplinary Graduate School of Engineering Sciences, Kyushu University, Kasuga, Fukuoka 816-8580, Japan*
[2]*Department of Physical Electronics, School of Electrical Engineering, Faculty of Engineering, Tel Aviv University, Tel Aviv 69978, Israel*
(Received 3 December 2010; revised manuscript received 4 February 2011; published 29 March 2011)

We revisit the problem of the spontaneous symmetry breaking (SSB) of solitons in two-component linearly coupled nonlinear systems, adding the nonlinear interaction between the components. With this feature, the system may be realized in new physical settings, in terms of optics and the Bose-Einstein condensate (BEC). SSB bifurcation points are found analytically, for both symmetric and antisymmetric solitons (the symmetry between the two components is meant here). Asymmetric solitons, generated by the bifurcations, are described by means of the variational approximation (VA) and numerical methods, demonstrating good accuracy of the variational results. In the space of the self-phase-modulation (SPM) parameter and soliton's norm, a border separating stable symmetric and asymmetric solitons is identified. The nonlinear coupling may change the character of the SSB bifurcation, from subcritical to supercritical. Collisions between moving asymmetric and symmetric solitons are investigated too. Antisymmetric solitons are destabilized by a supercritical bifurcation, which gives rise to self-confined modes featuring Josephson oscillations, instead of stationary states with broken antisymmetry. An additional instability against delocalized perturbations is also found for the antisymmetric solitons.

DOI: 10.1103/PhysRevE.83.036608 PACS number(s): 05.45.Yv, 03.75.Lm, 42.65.Tg, 47.20.Ky

## I. INTRODUCTION

Spontaneous symmetry breaking (SSB) is a fundamental feature of two-core physical systems, originating from the competition of the linear tunnel coupling between the cores and nonlinearity acting inside each of them. The possibility of this effect was originally demonstrated in Ref. [1]. The first physical setting where the SSB was studied in detail theoretically is represented by dual-core optical fibers, in which this effect was predicted for continuous-wave states [2] and solitons [3–5]. Later, the analysis of the SSB was extended to Bose-Einstein condensates (BECs) trapped in symmetric double-well potentials, in the framework of both the quantum [6,7] and mean-field [8] descriptions. In the experiment, the SSB has been experimentally demonstrated in the condensate of $^{87}$Rb atoms with the self-repulsive nonlinearity [12]. In the settings with the attractive or repulsive intrinsic nonlinearity, stationary asymmetric modes are generated by SSB *bifurcations* from symmetric and antisymmetric states, respectively. In the framework of the mean-field theory, the analysis of the SSB in nonlinear matter waves was extended for two-dimensional solitons, supported by the combination of the self-attractive [9,10] or self-repulsive [10,11] nonlinearity and periodic optical-lattice potentials. The SSB was also studied in settings based on double-well nonlinear *pseudopotentials* [15], optical models with the cubic-quintic nonlinearity acting inside the linearly-coupled cores (which gives rise to closed bifurcation loops) [16], dipolar BECs [17], two- [13] and three-component (spinor) [14] BEC mixtures, and Bose-Fermi mixtures [18].

An effect related to the SSB is Josephson oscillations in BEC trapped in double-well potentials. After the prediction of the oscillations in Ref. [19], they were observed in various experimental settings [12,20]. Further theoretical aspects of the Josephson oscillations were investigated too [21], including the oscillations of solitons [22] (similar oscillations of solitons in dual-core nonlinear optical fibers were studied earlier in Ref. [23]).

As mentioned above, in the theoretical studies of the SSB the emphasis was made on effects produced by the competition between the intercore linear coupling and intracore nonlinearities. A straightforward problem which was not studied yet is the modification of the SSB scenarios in solitons in cases when the two wave fields are coupled through both linear and nonlinear interactions. This extension makes it possible to predict SSB effects in new physical settings. In optics, these are waves with orthogonal polarizations propagating in a single-mode nonlinear fiber, the linear coupling between them being induced by the twist of the fiber or elliptic deformation of the core, in the cases of the linear and circular polarizations, respectively, while the nonlinear coupling between the polarizations is accounted for, as usual, by the XPM (cross-phase-modulation) terms [4]. In BEC, a similar model applies to a binary mixture of two different atomic states, with the linear interconversion between them imposed by a resonant radio-frequency electromagnetic wave [25], or by the two-photon Raman transition [26], while the XPM nonlinearity is generated, as usual, by interatomic collisions [24].

The objective of this work is to study the SSB bifurcations of symmetric and antisymmetric one-dimensional solitons in the two-component model with the self-focusing nonlinearity, combining the linear and XPM interaction terms, and analyze properties of asymmetric solitons generated by the bifurcations. The symmetry, antisymmetry, and asymmetry are meant with respect to the two components, rather than in the sense of the spatial parity—all the solitons considered here are even localized modes, except for moving antisymmetric solitons destabilized by delocalized perturbations (see Fig. 7 below). In Sec. II, we introduce the models and apply analytical methods, which allow us to find the bifurcation points in an exact form, and describe the bifurcations and solitons generated by them by dint of the variational approximation (VA). The VA

 

is also applied to the description of oscillations developed by unstable solitons, showing, in all cases, good accuracy in comparison with numerical results, which are reported in Sec. III. A border between stable symmetric and antisymmetric solitons is identified, and it is found that the addition of the XPM interactions may change the character of the SSB bifurcation for symmetric solitons from subcritical to supercritical. Asymmetric-asymmetric and asymmetric-symmetric collisions between moving stable solitons are also studied by means of direct simulations, demonstrating both quasielastic and strongly inelastic outcomes. In the case of antisymmetric solitons, the SSB bifurcation is supercritical. An additional mechanism of the destabilization of antisymmetric solitons may be triggered by delocalized (expanding) perturbations. Results obtained in this work are summarized in Sec. IV.

## II. ANALYTICAL RESULTS

### A. The model

We consider the two-component Gross-Pitaevskii/nonlinear Schrödinger equations in one dimension, in the scaled form:

$$\begin{aligned} i\phi_t &= -(1/2)\phi_{xx} - (\varepsilon|\phi|^2 + |\psi|^2)\phi - \psi, \\ i\psi_t &= -(1/2)\psi_{xx} - (\varepsilon|\psi|^2 + |\phi|^2)\psi - \phi. \end{aligned} \tag{1}$$

The equations are written in the notation corresponding to the BEC, with $\hbar = m = 1$ (this scaling is possible because masses of two hyperfine atomic states coupled by the linear conversion are always equal). The linear-coupling and XPM coefficients are also scaled to be 1, which is always possible (setting the XPM coefficient equal to $+1$, in the present notation, means that the interatomic interactions are attractive), while the SPM (self-phase-modulation) coefficient, $\varepsilon$, is the single irreducible parameter of the system.

In the most general case, the SPM coefficients in the two equations may be different, $\varepsilon_\phi \neq \varepsilon_\psi$, if the scattering lengths for collisions between atoms in the two states are unequal. In this paper, we aim to consider the symmetric system, with the single coefficient $\varepsilon$. Actually, $\varepsilon$ may be readily adjusted by means of the Feshbach-resonance technique [27].

The number of atoms in the condensate is proportional to the total norm of the wave function,

$$N = \int_{-\infty}^{+\infty} [|\phi(x)|^2 + |\psi(x)|^2]dx. \tag{2}$$

The comparison with the Gross-Pitaevskii equations written in physical units demonstrates that $N = 1$ corresponds (for instance) to $\sim$1000 atoms in the $^7$Li condensate (with the scattering length $\sim -0.1$ nm), confined in the transverse plane by the harmonic-oscillator potential with frequency $\sim$100 Hz [28].

In the application to optics, variables $t$ and $x$ are replaced by the propagation distance and reduced time ($z$ and $\tau$, in the standard notation), the signs in front of the second derivatives corresponding to the anomalous group-velocity dispersion in the optical fiber [4]. In the standard model of optical fibers, $\varepsilon = 3/2$ for linear polarizations, and $\varepsilon = 1/2$ for circular polarizations. Other values of $\varepsilon$ are possible too, in photonic-crystal fibers [29].

Stationary solutions to Eqs. (1) with chemical potential $\mu$ are looked for in the usual form, $\{\phi(x,t),\psi(x,t)\} = e^{-i\mu t}\{u(x),v(x)\}$, where real functions $u$ and $v$ satisfy equations

$$\begin{aligned} \mu u &= -(1/2)u'' - (\varepsilon u^2 + v^2)u - v, \\ \mu v &= -(1/2)v'' - (\varepsilon v^2 + u^2)v - u. \end{aligned} \tag{3}$$

The chemical potentials of the two components may only be equal in the presence of the linear coupling between them.

### B. Exact results for the bifurcation points

Obvious exact solutions to Eqs. (3) are symmetric and antisymmetric solitons:

$$u_{\rm sol}(x) = \pm v_{\rm sol}(x) = A\,{\rm sech}(x/W), \tag{4}$$

with amplitude $A$ and the chemical potentials given by

$$A = 1/(W\sqrt{1+\varepsilon}), \quad \mu_\pm = -1/(2W^2) \mp 1, \tag{5}$$

provided that $\varepsilon > -1$. Norm (2) of these solutions is

$$N = 4(1+\varepsilon)^{-1}W^{-1}. \tag{6}$$

It is possible to find the exact position of bifurcation points which are responsible for the emergence of asymmetric solitons from the symmetric and antisymmetric ones, following the known approach [3,5]. To this end, in the case of the symmetric soliton, one substitutes the following perturbed expressions into Eqs. (3):

$$\{\tilde{u}(x),\tilde{v}(x)\}_{\rm symm} = \{u_{\rm sol}(x) + \delta u(x), \quad u_{\rm sol}(x) - \delta u(x)\}, \tag{7}$$

with the infinitesimal antisymmetric perturbation, $\{\delta u(x), -\delta u(x)\}$, which accounts for the onset of the SSB bifurcation. Similarly, in the case of the antisymmetric soliton, one substitutes

$$\{\tilde{u}(x),\tilde{v}(x)\}_{\rm anti} = \{u_{\rm sol}(x) + \delta u(x), \quad -u_{\rm sol}(x) + \delta u(x)\}, \tag{8}$$

where the spontaneous breaking of the *antisymmetry* is accounted for by the *symmetric* perturbation, $\{\delta u(x),\delta u(x)\}$. In either case, the linearization of Eq. (3) with respect to perturbations (7) or (8) yields the respective equation for the perturbation mode,

$$(\mu \pm 1)\delta u = -\left[\frac{1}{2}\frac{d^2}{dx^2} + (3\varepsilon - 1)A^2{\rm sech}^2\left(\frac{x}{W}\right)\right]\delta u, \tag{9}$$

where the upper and lower signs pertain to the symmetric and antisymmetric solitons, respectively, and expression (4) was substituted for the soliton's wave form.

The actual bifurcation of the symmetric or antisymmetric soliton takes place when Eq. (9) has a nontrivial localized solution, i.e., the respective small symmetry-(or antisymmetry-) breaking perturbation represents a true eigenmode with the zero eigenvalue (the zero mode is the signature of the corresponding phase transition). In fact, Eq. (9) is well known in quantum mechanics, with term $-(3\varepsilon - 1)A^2{\rm sech}^2(x/W)$ representing a potential well (provided that $\varepsilon > 1/3$). According to the results from quantum mechanics, Eq. (9) gives rise

to localized solutions (bound states) at the following discrete values of the chemical potential:

$$\mu \pm 1 = -\frac{1}{8W^2}[-(1+2n) + \sqrt{1+8(3\varepsilon-1)A^2W^2}]^2, \tag{10}$$

with integer $n$ taking values $n = 0,1,2,...$, limited by condition

$$n < \frac{1}{2}[\sqrt{1+8(3\varepsilon-1)A^2W^2} - 1].$$

Using Eqs. (5) and (2) to eliminate $W$, $\mu$ and $A$ in favor of $N$, we obtain from Eq. (10) with $n = 0$ (which corresponds to the ground state in the quantum-mechanical problem) an eventual result for the norm of the symmetric soliton at the critical (bifurcation):

$$N_c^2 = \frac{256(\varepsilon+1)^{-1}}{(\sqrt{25\varepsilon-7} - 3\sqrt{\varepsilon+1})(\sqrt{25\varepsilon-7} + \sqrt{\varepsilon+1})}. \tag{11}$$

Expression (11) is positive (i.e., the bifurcation really occurs for the symmetric solitons) at $\varepsilon > 1$.

For the *antisymmetry-breaking* bifurcation, the consideration demonstrates that the bound-state solution for $\delta u$ exists at the point which differs from its counterpart for the symmetric solitons by the opposite sign in Eq. (11):

$$N_c^2 = -\frac{256(\varepsilon+1)^{-1}}{(\sqrt{25\varepsilon-7} - 3\sqrt{\varepsilon+1})(\sqrt{25\varepsilon-7} + \sqrt{\varepsilon+1})}. \tag{12}$$

This expression is positive at $\varepsilon < 1$. On the other hand, the above analysis makes sense if the last term in Eq. (9) represents the potential well (rather than a barrier), i.e., at $\varepsilon > 1/3$, hence the bifurcation of the antisymmetric solitons occurs in the interval of $1/3 < \varepsilon < 1$. It is worth mentioning that in the case of $\varepsilon = 1$, when the bifurcation is absent, Eqs. (1) with the linear-coupling terms represent an integrable system [30], unlike the situation at $\varepsilon \neq 1$.

### C. The variational approximation: stationary modes

Except for the identification of the bifurcation points, exact results for asymmetric solitons are not available, hence the VA (variational approximation) should be used [5]. To this end, we note that the Lagrangian of corresponding to Eqs. (1) is

$$\begin{aligned} L = \frac{1}{2}\int_{-\infty}^{\infty} [&i(\phi_t\phi^* - \phi_t^*\phi + \psi_t\psi^* - \psi_t^*\psi) \\ &- (|\phi_x|^2 + |\psi_x|^2) + \varepsilon(|\phi|^4 + |\psi|^4) + |\phi|^2|\psi|^2 \\ &+ 2(\phi^*\psi + \phi\psi^*)]dx. \end{aligned}$$

If the *ansatz* for solitons is adopted in the form of

$$\phi = A\,\mathrm{sech}(x/W)\exp(-i\mu t), \psi = B\,\mathrm{sech}(x/W)\exp(-i\mu t), \tag{13}$$

the Lagrangian is evaluated as

$$\begin{aligned} 2L_{\rm eff} = &\mu W(A^2+B^2) - (1/6)W^{-1}(A^2+B^2) \\ &+ (1/3)\varepsilon W(A^4+B^4) + (2/3)WA^2B^2 + 2WAB, \end{aligned} \tag{14}$$

the corresponding total norm being

$$N = 2W(A^2+B^2). \tag{15}$$

If the asymmetry measure of the soliton, $r$, is defined as

$$\begin{aligned} \Delta N \equiv \int_{-\infty}^{+\infty} dx(|\phi|^2 - |\psi|^2) = 2W(A^2-B^2), \\ r \equiv \frac{\Delta N}{N} = \frac{A^2-B^2}{A^2+B^2}, \end{aligned} \tag{16}$$

Lagrangian (14) can be cast into the following form:

$$\begin{aligned} L_{\rm eff} = \frac{N}{4}\Bigg[&\mu - \frac{1}{6W^2} + \frac{\varepsilon N}{12W}(1+r^2) \\ &+ \frac{N}{12W}(1-r^2) \pm \sqrt{1-r}\Bigg]. \end{aligned}$$

Here $\pm$ designates the sign of $AB$, i.e., the relative sign of the two fields, as per Eq. (13). Then, the following system of the Euler-Lagrange equations is derived from the variational principle [5]:

$$\begin{aligned} \frac{\partial L_{\rm eff}}{\partial N} \equiv \frac{\mu}{2} - \frac{1}{12W^2} + \frac{(\varepsilon+1)N}{12W} \pm \frac{1}{2\sqrt{1-r^2}} = 0, \\ \frac{1}{N^2}\frac{\partial L_{\rm eff}}{\partial r} \equiv r\left[\frac{(\varepsilon-1)}{12W} \mp \frac{1}{2N\sqrt{1-r^2}}\right] = 0, \end{aligned} \tag{17}$$

$$\frac{\partial L_{\rm eff}}{\partial W} \equiv \frac{1}{6}\left[\frac{N}{W} - \frac{\varepsilon N^2}{4}(1+r^2) - \frac{N^2}{4}(1-r^2)\right] = 0. \tag{18}$$

The soliton's width $W$ is found from Eq. (18),

$$\frac{1}{W} = \frac{N}{4}[1+\varepsilon-(1-\varepsilon)r^2], \tag{19}$$

while asymmetry ratio $r$ is a solution to the equation which then follows from Eq. (17):

$$\frac{(\varepsilon-1)N}{24}[(1+\varepsilon)-(1-\varepsilon)r^2] = \frac{\pm 1}{N\sqrt{1-r^2}}. \tag{20}$$

Near the bifurcation point $r$ is small, hence one may use the expansion, $(1-r^2)^{-1/2} \approx 1 + (1/2)r^2$ in Eq. (20), which yields

$$r^2 \approx \frac{N^2(\varepsilon^2-1) \mp 24}{\pm 12 - N^2(\varepsilon-1)^2}. \tag{21}$$

The critical value $\varepsilon_c$, at which $r^2$ vanishes (the bifurcation point), is given by

$$\varepsilon_c(N) = \sqrt{1 \pm 24/N^2}. \tag{22}$$

In fact, Eq. (22) is a variational counterpart of exact relations (11) and (12) which determine the point of the symmetry- or antisymmetry-breaking bifurcation. Comparison between the exact (solid curves) and variational (dashed curves) relations is shown below in Figs. 1(c) and 6(c).

For $AB > 0$, i.e., for the asymmetric solitons originating from the symmetric one at $\varepsilon > 1$ (as shown above), Eq. (21) with the upper signs yields a relevant result, $r^2 > 0$, at $\varepsilon > \varepsilon_c(N)$ for $N > \sqrt{3}$, and at $\varepsilon < \varepsilon_c(N)$ for $N < \sqrt{3}$. On the other hand, for $AB < 0$, i.e., for the solitons originating form the antisymmetric one at $\varepsilon < 1$, Eq. (21) with the lower signs yields $r^2 > 0$ at $-\varepsilon_c < \varepsilon < \varepsilon_c$ for $N > 2\sqrt{6}$.

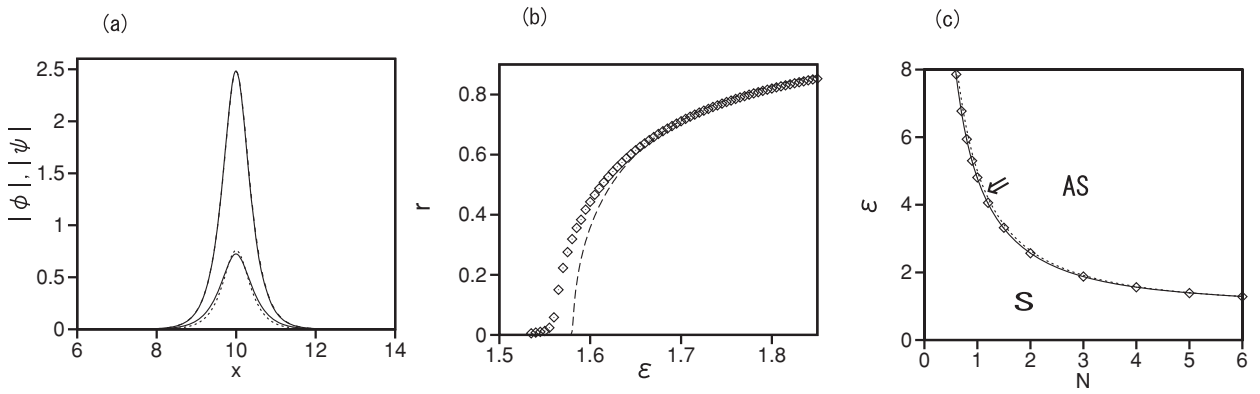


FIG. 1. (a) The continuous and dashed curves depict asymmetric solitons for $N = 4$ and $\varepsilon = 1.8$, as obtained in the numerical form and predicted by the VA, respectively. (b) The bifurcation diagram, in the form of the asymmetry parameter, $r$ [defined as per Eq. (16)], versus the SPM coefficient, $\varepsilon$, for a fixed norm, $N = 4$. (c) The border between symmetric (**S**) and asymmetric (**AS**) solitons in the $(N,\varepsilon)$ plane. The solid line denotes the exact analytical result given by Eq. (11). In panels (b) and (c), chains of rhombuses and the dashed curve show, severally, numerical results and predictions of the VA. The arrow in (c) indicates the border between the subcritical and supercritical bifurcations, as identified from the numerical results, see the text.

The VA may also predict the type of the SSB bifurcation, subcritical or supercritical [i.e., with the corresponding curves $r(N)$ for the asymmetric-soliton family that do or do not feature turning points, at which $dN/dr = 0$ [3,5]. Differentiating Eq. (20) with respect to $r$ and substituting $dN/dr = 0$, after simple manipulations we arrive at the following relation which must hold at the turning point:

$$r^2 = (1/3)(\varepsilon - 3)/(\varepsilon - 1). \tag{23}$$

Obviously, the turning point exists (within the framework of the VA) if Eq. (23) yields $r^2 > 0$, which takes place at $\varepsilon > 3$, i.e., for the asymmetric solitons emerging from the symmetric ones, if $\varepsilon$ is large enough (in accordance with the above-mentioned fact that, in the model without the XPM interaction, i.e., at $\varepsilon \to \infty$, the bifurcation of the symmetric soliton is always subcritical [3,5]). Further, the condition $\varepsilon_c > 3$, if substituted into Eq. (22) with the upper sign, gives $N < \sqrt{3}$, hence the bifurcation of the symmetric soliton is subcritical if it happens at $N < N_0 \equiv \sqrt{3}$, and supercritical in the opposite case.

Thus, the addition of the XPM nonlinearity to the two-component system may transform the corresponding SSB bifurcation from subcritical into supercritical. It is relevant to mention that a similar effect is produced, in the absence of the XPM terms, by the periodic (optical-lattice) potential [11].

### D. The variational approximation: Dynamics

To consider the dynamics of nonstationary solitons within the framework of the VA, we assume a generalized *ansatz* [cf. Eq. (13)], $\phi = A\ \mathrm{sech}(x/W)\exp[-i\theta_1(t)], \psi = B\mathrm{sech}(x/W)\exp[-i\theta_2(t)]$, with time-dependent phases $\theta_{1,2}(t)$. In this case, the effective Lagrangian is evaluated as

$$\begin{aligned} 2L_{\mathrm{eff}} = N[&(1/4)(\dot\theta_1 + \dot\theta_2) + (r/4)(\dot\theta_1 - \dot\theta_2) - (1/12)W^{-2} \\ &+ (\varepsilon/24)NW^{-1}(1 + r^2) + (N/24)W^{-1}(1 - r^2) \\ &\pm (1/2)\sqrt{1 - r}\cos(\theta_1 - \theta_2)], \end{aligned}$$

with the overdot standing for the time derivative. Accordingly, the time evolution of $r$ and $\Delta\theta \equiv \theta_1 - \theta_2$ is governed by the following variational equations:

$$\frac{dr}{dt} = \mp 2\sqrt{1 - r^2}\sin(\Delta\theta),$$

$$\begin{aligned} \frac{d}{dt}\Delta\theta = 2\Bigg\{ &\frac{\pm r}{\sqrt{1 - r^2}}\cos(\Delta\theta) \\ &- \frac{N^2}{24}[(\varepsilon^2 - 1)r + (\varepsilon - 1)^2 r^3]\Bigg\}. \end{aligned} \tag{24}$$

## III. NUMERICAL RESULTS AND VERIFICATION OF THE VARIATIONAL APPROXIMATION

### A. Symmetric and asymmetric solitons

Proceeding to the presentation of numerical results, we first consider the symmetric solitons and their SSB instability. Soliton solutions were generated by means of the imaginary-time integration of Eqs. (1), which produces the ground (lowest-energy) state. Figure 1(a) shows soliton profiles for $N = 4$ and $\varepsilon = 1.8$. The solid lines display the numerical solutions (the taller and lower ones are $|\phi|$ and $|\psi|$, respectively), and the dashed curves represents the predictions of the VA for the same values of parameters, which are $|\phi(x)| = 2.47\mathrm{sech}[(x - 10)/0.299]$ and $|\psi(x)| = 0.76\mathrm{sech}[(x - 10)/0.299]$, as per Eqs. (13), (15), (16) ), ((19), and (20). The taller profile is very well approximated by the VA, with a slight discrepancy observed for the lower one. The stability of symmetric solitons generated by the (obviously, supercritical) bifurcation in this case was verified by direct simulations of Eqs. (1).

Figure 1(b) shows the bifurcation diagram, in the form of the asymmetry measure $r$ [see Eq. (16)] as a function of $\varepsilon$ for $N = 4$, along with the VA-predicted counterpart of this dependence. Further, Fig. 1(c) displays the phase diagram for the symmetric and asymmetric solitons in the $(N,\varepsilon)$ plane. The numerically identified bifurcation is *supercritical* for $N > N_0 \approx 1.15$, and weakly *subcritical* for $N < N_0$ [the border between these types

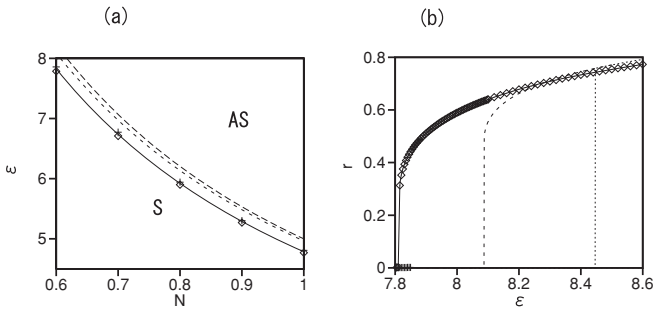


FIG. 2. (a) A blowup of the diagram from Fig. 1(c) for $N < 1$ (in the region where the symmetry-breaking bifurcation is slightly subcritical). (b) The same as in Fig. 1(b), but for $N = 1$. In (a), the solid curve represents the exact result given by Eq. (11), the closely set dashed curves delineate a narrow bistability region, as predicted by the VA, and two almost overlapping sets of symbols represent a tiny bistability region as produced by the numerical results. In (b), two nearly vertical dashed lines depict the VA-predicted hysteresis (bistability).

is indicated by the arrow in Fig. 1(c)]. The above-mentioned prediction produced by the VA for the border between the sub- and supercritical bifurcations, $N_0 = \sqrt{3}$, is reasonably close to the observation elicited from the numerical data.

Additional comparison of the numerical and variational results is presented in Fig. 2. In particular, (a) shows a zoom of the tiny mismatch between the numerical and VA-predicted borders separating symmetric and asymmetric solitons in Fig. 1(c) at $N < 1$, and Fig. 2(b) shows $r$ as a function of $\varepsilon$ for $N = 1$. A very weak hysteresis (bistability) is observed in the numerical results displayed in the latter panel at $7.815 < \varepsilon < 7.850$, owing to the weakly subcritical character of the bifurcation. In this respect, the VA is less accurate, predicting a much broader and shifted hysteretic region between the nearly vertical dashed lines in Fig. 2(b).

Direct simulations of Eqs. (1) corroborate the stability of the asymmetric solitons generated by the bifurcation, and the instability of the symmetric soliton past the bifurcation point. In particular, the continuous curve in Fig. 3(a) shows the

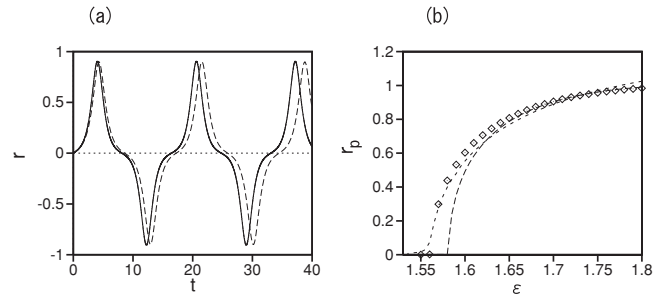


FIG. 3. (a) The continuous curve displays the evolution of the asymmetry parameter $r$ in oscillations of the unstable symmetric soliton, with $N = 4$ and $\varepsilon = 1.7$, as obtained from direct simulations. The dashed curve is the same, as predicted by the variational equation (24). (b) The peak value (amplitude) $r_p$ of $r(t)$ versus $\varepsilon$ for $N = 4$ (see further explanations in the text).

temporal evolution of the asymmetry measure $r$ as produced by the simulations of Eqs. (1) with initial conditions

$$\begin{aligned}\phi_0(x) &= A\,\mathrm{sech}[(x - L/2)/W]\exp(0.01i), \psi \\ &= A\,\mathrm{sech}[(x - L/2)/W]\exp(-0.01i),\end{aligned} \tag{25}$$

where the amplitude and width, $A = 1/(W\sqrt{1+\varepsilon})$ and $W = 4/[N(1+\varepsilon)]$, are taken as per the exact solution for the symmetric soliton, see Eqs. (4) and (2) ($x = L/2$ is the central point of the integration domain), for $N = 4$ and $\varepsilon = 1.7$. The small phase shift between the two components in expression (25), $\Delta\Phi = -0.02$, triggers the onset of the instability of the symmetric soliton past the bifurcation point. The simulations demonstrate that $r(t)$ oscillates between $-0.903$ and $+0.903$. For comparison, the dashed curve in Fig. 3(a) shows the evolution of $r(t)$ produced by simulations of variational equations (24), with the corresponding initial conditions: $r_0 = 0$ and $\Delta\theta_0 = -0.02$.

Note that the peak value (amplitude) of $r$ in the oscillatory regime is $r_p = 0.903 \approx 1.27 \times r_{\rm st}$, where $r_{\rm st} = 0.711$ is the value of $r$ for the stationary asymmetric soliton, with the same $N$ and $\varepsilon$. The chain of symbols in Fig. 3(b) shows numerically found amplitudes $r_p$ for the oscillations starting from the same initial conditions (25) with other values of $\varepsilon$ and $N = 4$. The long-dashed line in the same figure is the prediction for $r_p$ produced by Eqs. (24), while the short-dotted curve is a phenomenological fitting, $1.25 \times r_{\rm st}$, where $r_{\rm st}$ is the aforementioned asymmetry parameter of the numerically found stationary solitons. Thus, one may conclude that the VA produces results similar to their numerical counterparts in the dynamical regime too.

### B. Collisions between asymmetric solitons

The availability of the stable asymmetric solitons suggests to study interactions between moving ones, cf. Ref. [31]. We have performed simulations of collisions between two identical asymmetric solitons, which were set in motion with velocities $\pm k$ by applying the kicks to them, i.e., multiplying the wave function of each soliton by $\exp(\pm ikx)$. Typical results are displayed in Fig. 4. For small and large velocities, $k = 0.1$ and $k = 0.5$, the collisions are quasielastic, with the difference that the slowly moving solitons, with $k = 0.1$, bounce from each other, while fast solitons, with $k = 0.5$, pass through each other. On the other hand, in Fig. 4(b) the collision is clearly inelastic for an intermediate velocity, $k = 0.3$.

Further, Fig. 5 displays results for the collisions between the asymmetric soliton with $N = 4$ and symmetric one, with $N = 2$ and $\varepsilon = 1.8$. In the case of $k = 0.1$, the solitons demonstrate mutual repulsion (therefore the collision is quasi-elastic), while they overcome the repulsion and merge into a single soliton at $k = 0.5$. At a still larger velocity, $k = 1$, the solitons pass through each other. Thus, strongly inelastic interactions are observed in the intermediate range of velocities in both cases shown in Figs. 4 and 5.

### C. Antisymmetric solitons

According to Eq. (22), the VA predicts that the antisymmetric solitons undergo a bifurcation at $N^2 = 24$, in the range of $1/3 < \varepsilon < 1$ (see the previous section). Accordingly, the

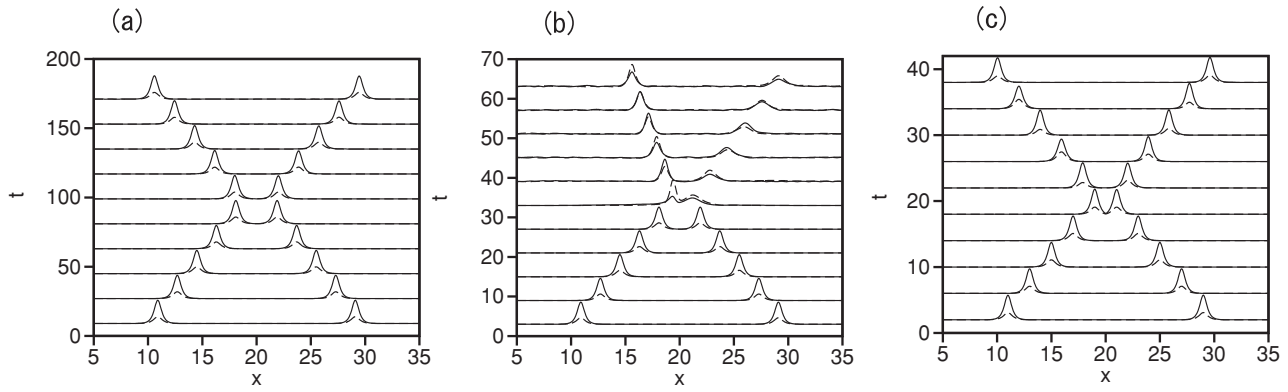


FIG. 4. Collisions between two asymmetric solitons with $N = 4$ at $\varepsilon = 1.8$. The initial velocities are $k = \pm 0.1$ (a), $k = \pm 0.3$ (b), and $k = \pm 0.5$ (c).

antisymmetric soliton is expected to be unstable at $N^2 > 24$, and may be replaced by a nontrivial mode with broken antisymmetry. However, the imaginary-time-integration method fails to generate such stationary asymmetric solitons. On the other hand, it is easy to test the expected instability of the antisymmetric solitons at $N^2 > 24$ in direct real-time simulations. To this end, we have performed simulations of Eq. (1), starting with the following initial conditions:

$$\begin{aligned} \phi_0(x) &= -A\,\mathrm{sech}[(x - L/2)/W]\exp(0.01i), \\ \psi_0(x) &= A\,\mathrm{sech}[(x - L/2)/W]\exp(-0.01i), \end{aligned} \tag{26}$$

with $A = 1/(W\sqrt{1+\varepsilon})$ and $W = 4/[N(1+\varepsilon)]$, where the phase shift between the two fields, $\Delta\Phi = -0.02$, plays the role of the initial perturbation, cf. Eq. (25). As an example, the continuous curve in Fig. 6(a) shows the resulting evolution of the asymmetry parameter, $r(t)$, for $N = 8$ and $\varepsilon = 0.75$. Large-amplitude oscillations of $r(t)$ make it evident that the initial antisymmetric soliton with $r = 0$ is unstable indeed. The dashed curve in Fig. 6(a) displays results which were produced, for the same case, by variational equations (24). In fact, these figures display Josephson oscillations of the soliton, cf. Refs. [22].

In Fig. 6(b), the chain of rhombuses shows the peak amplitude, $r_p$, of the oscillations of $r(t)$ versus $\varepsilon$. In parallel, the dashed line shows the same amplitude as predicted by Eqs. (24). The picture suggests that a supercritical bifurcation from the antisymmetric solitons to the oscillatory mode (instead of the transition to a stationary state with broken antisymmetry) occurs near $\varepsilon = 0.785$. The critical line for the bifurcation in the plane of $(N,\varepsilon)$, as obtained from the numerical data, is drawn as the chain of rhombuses in Fig. 6(c). The solid curve denotes the exact bifurcation points given by Eq. (11), and the dashed curve in the same figure is the critical line $\varepsilon_c = \sqrt{1 - 24/N^2}$, as predicted by the VA, see Eq. (22).

In the direct simulations, the antisymmetric solitons are stable above the critical curve in Fig. 6(c) for $N > 6$. However, there is another instability mode for the antisymmetric solitons, found at $N < 6$, for $\varepsilon < \tilde{\varepsilon}_c$ with some new critical value $\tilde{\varepsilon}_c$. Figure 7(a) illustrates the manifestation of this instability for $N = 5$ and $\varepsilon = 0.74$. The initial conditions in this case were taken with a very small difference between the amplitudes of the two components of the soliton,

$$\begin{aligned} \phi_0(x) &= -1.001A\,\mathrm{sech}[(x - L/2)/W], \\ \psi_0(x) &= 0.999A\,\mathrm{sech}[(x - L/2)/W], \end{aligned}$$

again with $A = 1/(W\sqrt{1+\varepsilon})$ and $W = 4/[N(1+\varepsilon)]$, cf. Eqs. (25) and (26). This instability breaks the antisymmetry and sets the soliton into motion.

To study this instability in detail, we used the corresponding Bogoliubov–de Gennes equations,

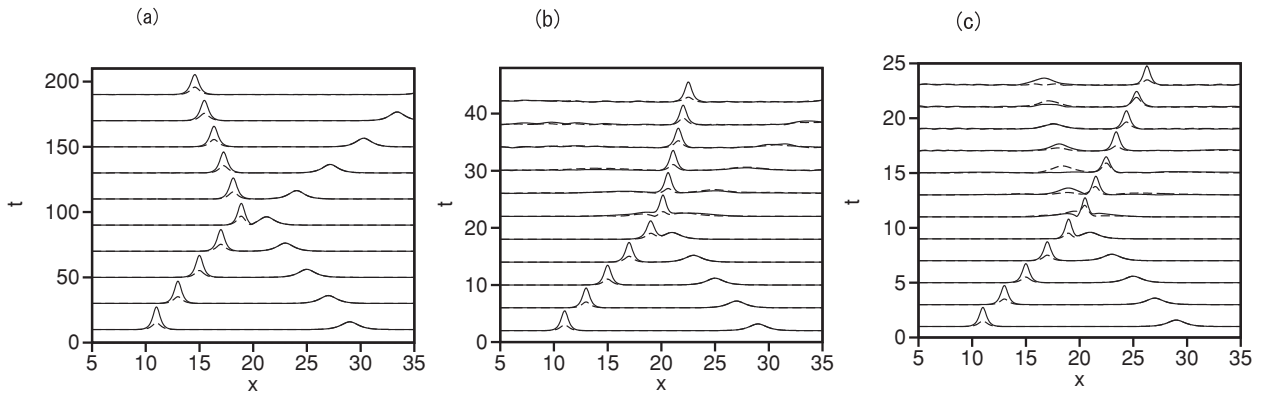


FIG. 5. Collisions between asymmetric and symmetric solitons (with $N = 4$ and $N = 2$, respectively), at $\varepsilon = 1.8$. The initial velocities are $k = \pm 0.1$ (a), $k = \pm 0.5$ (b), and $k = \pm 1$ (c).

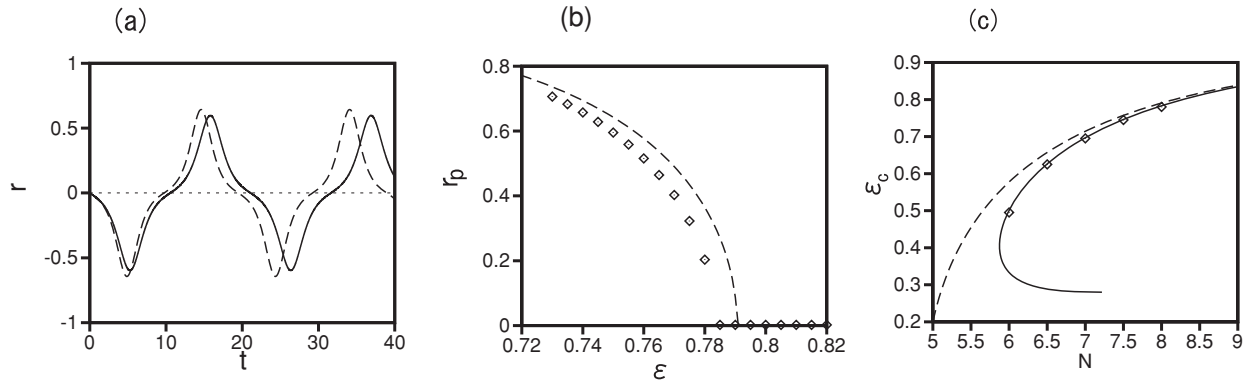


FIG. 6. (a) The continuous curve shows the evolution of $r(t)$ for the unstable antisymmetric soliton, produced by direct simulations at $N = 8$ and $\varepsilon = 0.75$. The dashed curve displays the same result, as produced by simulations of variational equation (24). (b) Rhombuses and the dashed line depict the peak value (amplitude) of $r(t)$, as found, respectively, from the direct simulations and predicted by Eq. (24). (c) The stability border for the antisymmetric solitons, as revealed by the direct simulations (rhombuses) and predicted by the VA (the dashed line). The solid curve in panel (c) depicts the exact analytical result as per Eq. (11).

i.e., the linearization of Eqs. (1) for perturbations $\{\delta\phi(x,t),\delta\psi(x,t)\}$ around the antisymmetric soliton, $\phi = -\psi \equiv \phi_0 = A\,\mathrm{sech}(x/W)\exp(-i\mu_- t)$, see Eq. (4):

$$\begin{aligned} i(\delta\phi)_t &= -(1/2)(\delta\phi)_{xx} - (2\varepsilon+1)|\phi_0|^2\delta\phi - \varepsilon\phi_0^2(\delta\phi)^* \\ &\quad + |\phi_0|^2\delta\psi + \phi_0^2(\delta\psi)^* - \delta\psi, \\ i(\delta\psi)_t &= -(1/2)(\delta\psi)_{xx} - (2\varepsilon+1)|\phi_0|^2\delta\psi - \varepsilon\phi_0^2(\delta\psi)^* \\ &\quad + |\phi_0|^2\delta\phi + \phi_0^2(\delta\phi)^* - \delta\phi. \end{aligned} \tag{27}$$

Equations (27) were solved by direct simulations, and the soliton's instability growth rate, $\lambda$, was extracted from the numerically found norm of the perturbation, $[S(t)]^2 \equiv \int_{-\infty}^{+\infty}[|\delta\phi(x,t)|^2 + |\delta\psi(x,t)|]^2 dx$ , fitting it to $S \approx \mathrm{const}\cdot\exp(\lambda t)$. The full instability eigenvalue is complex, as the instability is oscillatory, and the perturbation modes $\delta\phi$ and $\delta\psi$ are not localized, gradually expanding along $x$. Figure 7(b) shows the so found values of $\lambda$, for $N = 5$ and the system's size $L = 20$, as a function of $\varepsilon$. The instability sets in near $\varepsilon = 0.85$. Figure 7(c) shows the instability border, $\tilde{\varepsilon}_c(N)$. A possible reason for the apparent irregularity of the instability bo rder line in the latter figure may be an effect of the boundary conditions on the delocalized perturbation mode which accounts for this instability.

## IV. CONCLUSION

In this paper, we have revisited the problem of the SSB (spontaneous symmetry breaking) of one-dimensional solitons in two-component nonlinear systems with the linear coupling between the components. Examples of such systems are well known in nonlinear optics and BEC. Unlike the previous works, our analysis includes the nonlinear (XPM) interaction between the components, which makes it possible to realize the system in new physical settings, in optics and BEC alike. The results were obtained by means of analytical methods (in particular, the bifurcation points were found in the exact form) and numerical computations, which corroborate good accuracy provided by the VA (variational approximation), in both static and dynamical settings. The border separating stable symmetric and asymmetric solitons in the space of the SPM coefficient and soliton's norm was identified. An essential finding is that the addition of the XPM coupling may change the character of the SSB bifurcation of symmetric solitons from subcritical to supercritical. The bifurcation acting on the antisymmetric solitons generates dynamical localized states which feature

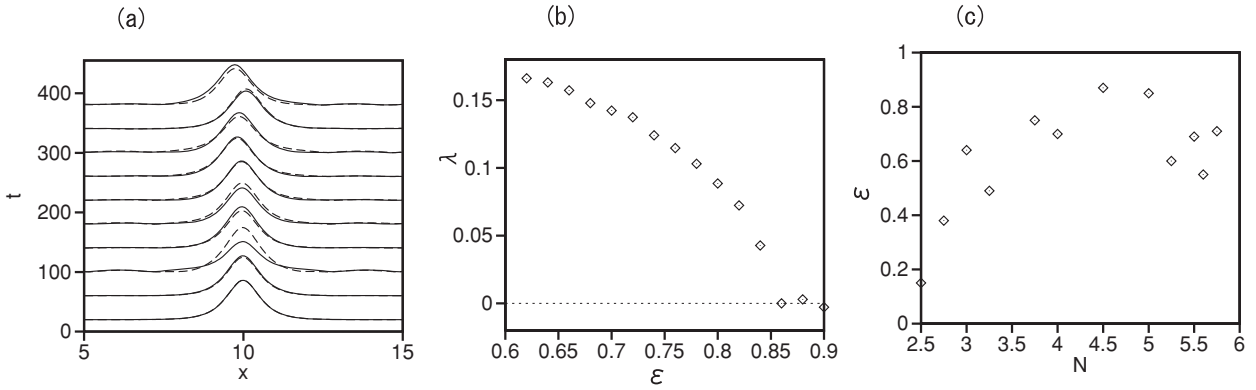


FIG. 7. (a) The evolution of $|\phi(x,t)|$ illustrating the instability of the antisymmetric soliton at $N = 8$ and $\varepsilon = 0.75$. (b) The corresponding numerically found instability growth rate versus $\varepsilon$. (c) The border of this instability, $\tilde{\varepsilon} = \varepsilon_c$, evaluated from the numerical solution of Eq. (27).

persistent Josephson oscillations, instead of stationary modes. An additional instability mode, induced by delocalized perturbations, was found for the antisymmetric solitons. Collisions between stationary solitons, asymmetric and symmetric ones, were explored by means of direct simulations, revealing both quasielastic and strongly inelastic outcomes.

Because periodic potentials (optical lattices) can also switch the character of the bifurcation from sub- to supercritical [11], it may be interesting to consider a more general model, in the form of Eq. (1) including the periodic potential, and study competition between the effects induced by the lattice potential and XPM nonlinearity, including the limit case of the SSB for discrete solitons in linearly coupled discrete nonlinear Schrödinger equations, cf. Ref. [32]. Another perspective extension may be to consider counterparts of these models in the two-dimensional geometry.


[1] E. B. Davies, Commun. Math. Phys. **64**, 191 (1979); J. C. Eilbeck, P. S. Lomdahl, and A. C. Scott, Physica D **16**, 318 (1985).

[2] W. Snyder, D. J. Mitchell, L. Poladian, D. R. Rowland, and Y. Chen, J. Opt. Soc. Am. B **8**, 2102 (1991).

[3] E. M. Wright, G. I. Stegeman, and S. Wabnitz, Phys. Rev. A **40**, 4455 (1989); C. Paré and M. Fłorjańczyk, *ibid*. **41**, 6287 (1990); A. I. Maimistov, Kvant. Elektron. **18**, 758 (1991) [Sov. J. Quantum Electron. **21**, 687 (1991)]; P. L. Chu, B. A. Malomed, and G. D. Peng, J. Opt. Soc. Am. B **10**, 1379 (1993); N. Akhmediev and A. Ankiewicz, Phys. Rev. Lett. **70**, 2395 (1993); B. A. Malomed, I. M. Skinner, P. L. Chu, and G. D. Peng, Phys. Rev. E **53**, 4084 (1996).

[4] G. P. Agrawal, *Nonlinear Fiber Optics* (Academic Press, San Diego, 1995).

[5] B. A. Malomed, in *Progress in Optics* edited by E. Wolf (North Holland, Amsterdam, 2002), Vol. 43, p. 71.

[6] G. J. Milburn, J. Corney, E. M. Wright, and D. F. Walls, Phys. Rev. A **55**, 4318 (1997).

[7] K. W. Mahmud, H. Perry, and W. P. Reinhardt, Phys. Rev. A **71**, 023615 (2005); C. Lee, Phys. Rev. Lett. **102**, 070401 (2009).

[8] A. Smerzi, S. Fantoni, S. Giovanazzi, and S. R. Shenoy, Phys. Rev. Lett. **79**, 4950 (1997); S. Raghavan, A. Smerzi, S. Fantoni, and S. R. Shenoy, Phys. Rev. A **59**, 620 (1999); E. Infeld, P. Zin, J. Gocalek, and M. Trippenbach, Phys. Rev. E **74**, 026610 (2006); G. Theocharis, P. G. Kevrekidis, D. J. Frantzeskakis, and P. Schmelcher, *ibid*. **74**, 056608 (2006); A. Gubeskys and B. A. Malomed, Phys. Rev. A **75**, 063602 (2007).

[9] M. Matuszewski, B. A. Malomed, and M. Trippenbach, Phys. Rev. A **75**, 063621 (2007).

[10] A. Gubeskys and B. A. Malomed, Phys. Rev. A **75**, 063602 (2007); T. Mayteevarunyoo and B. A. Malomed, J. Opt. A: Pure Appl. Opt. **11**, 094015 (2009); L. Gubeskys and B. A. Malomed, Phys. Rev. A **79**, 045801 (2009).

[11] M. Trippenbach, E. Infeld, J. Gocalek, M. Matuszewski, M. Oberthaler, and B. A. Malomed, Phys. Rev. A **78**, 013603 (2008).

[12] M. Albiez, R. Gati, J. Fölling, S. Hunsmann, M. Cristiani, and M. K. Oberthaler, Phys. Rev. Lett. **95**, 010402 (2005); R. Gati and M. Oberthaler, J. Phys. B **40**, R61 (2007).

[13] C. Wang, P. G. Kevrekidis, N. Whitaker, and B. A. Malomed, Physica D **327**, 2922 (2008); I. I. Satija, R. Balakrishnan, P. Naudus, J. Heward, M. Edwards, and C. W. Clark, Phys. Rev. A **79**, 033616 (2009); W. Wang, J. Phys. Soc. Jpn. **78**, 094002 (2009).

[14] C. Wang, P. G. Kevrekidis, N. Whitaker, T. J. Alexander, D. J. Frantzeskakis, and P. Schmelcher, J. Phys. A Math. Theor. **42**, 035201 (2009); B. Juliá-Diaz, M. Guilleumas, M. Lewenstein, A. Polls, and A. Sanpera, Phys. Rev. A **80**, 023616 (2009); B. Juliá-Diaz, M. Mele-Messeguer, M. Guilleumas, and A. Polls, *ibid*. **80**, 043622 (2009).

[15] L. C. Qian, M. L. Wall, S. Zhang, Z. Zhou, and H. Pu, Phys. Rev. A **77**, 013611 (2008); T. Mayteevarunyoo, B. A. Malomed, and G. Dong, *ibid*. **78**, 053601 (2008); C. Wang, P. G. Kevrekidis, N. Whitaker, D. J. Frantzeskakis, S. Middelkamp, and P. Schmelcher, Physica D **238**, 1362 (2009); N. V. Hung, P. Zin, M. Trippenbach, and B. A. Malomed, Phys. Rev. E **82**, 046602 (2010).

[16] L. Albuch and B. A. Malomed, Math. Comp. Simul. **74**, 312 (2007); Z. Birnbaum and B. A. Malomed, Physica D **237**, 3252 (2008); N. Dror and B. A. Malomed, *ibid*. **240**, 526 (2011).

[17] B. Xiong, J. Gong, H. Pu, W. Bao, and B. Li, Phys. Rev. A **79**, 013626 (2009).

[18] S. F. Caballero-Benítez, E. A. Ostrovskaya, M. Gulácsí, and Yu. S. Kivshar, J. Phys. B: At. Mol. Opt. Phys. **42**, 215308 (2009); S. K. Adhikari, B. A. Malomed, L. Salasnich, and F. Toigo, Phys. Rev. A **81**, 053630 (2010).

[19] J. Javanainen, Phys. Rev. Lett. **57**, 3164 (1986); M. W. Jack, M. J. Collett, and D. F. Walls, Phys. Rev. A **54**, R4625 (1996); I. Zapata, F. Sols, and A. J. Leggett, *ibid*. **57**, R28 (1998); M. J. Steel and M. J. Collett, *ibid*. **57**, 2920 (1998); S. Raghavan, A. Smerzi, S. Fantoni, and S. R. Shenoy, *ibid*. **59**, 620 (1999).

[20] F. S. Cataliotti, S. Burger, C. Fort, P. Maddaloni, F. Minardi, A. Trombettoni, A. Smerzi, and M. Inguscio, Science **293**, 843 (2001); T. Anker, M. Albiez, R. Gati, S. Hunsmann, B. Eiermann, A. Trombettoni, and M. K. Oberthaler, Phys. Rev. Lett. **94**, 020403 (2005); T. Zibold, E. Nicklas, C. Gross, and M. K. Oberthaler, *ibid*. **105**, 204101 (2010); S. Narayana and Y. Sato, *ibid*. **105**, 205302 (2010).

[21] V. M. Kaurov and A. B. Kuklov, Phys. Rev. A **73**, 013627 (2006); G. Mazzarella, M. Moratti, L. Salasnich, M. Salerno, and F. Toigo, J. Phys. B: At. Mol. Opt. Phys. **42**, 125301 (2009); K. Sakmann, A. I. Streltsov, O. E. Alon, and L. S. Cederbaum, Phys. Rev. Lett. **103**, 220601 (2009); J. Brand, T. J. Haigh, and U. Zulicke, Phys. Rev. A **80**, 011602 (2009); S. K. Adhikari, H. Lu, and H. Pu, *ibid*. **80**, 063607 (2009); M. Yasunaga and M. Tsubota, J. Low Temp. Phys. **158**, 51 (2010).

[22] M. Salerno, Laser Physics **15**, 620 (2005); C. Sudheesh, N. Bar-Gill, B. A. Malomed, and G. Kurizki, J. Phys. B: At. Mol. Opt. Phys. **43**, 205304 (2010); G. Mazzarella, B. Malomed, L. Salasnich, M. Salerno, and F. Toigo, *ibid*. **44**, 035301 (2011).

[23] P. L. Chu, B. A. Malomed, G. D. Peng, and I. M. Skinner, Phys. Rev. E **49**, 5763 (1994).

[24] R. J. Ballagh, K. Burnett, and T. F. Scott, Phys. Rev. Lett. **78**, 1607 (1997).

[25] S. K. Adhikari and B. A. Malomed, Phys. Rev. A **79**, 015602 (2009).
[26] M. Lewenstein, A. Sanpera, V. Ahufinger, B. Damski, A. Sen, and U. Sen, Adv. Phys. **56**, 243 (2007).
[27] C. Chin, R. Grimm, P. Julienne, and E. Tiesinga, Rev. Mod. Phys. **82**, 1225 (2010).
[28] K. E. Strecker, G. B. Partridge, A. G. Truscott, and R. G. Hulet, New J. Phys. **5**, 731 (2003).
[29] A. S. Cerqueira, Jr., Rep. Prog. Phys. **73**, 024401 (2010).
[30] M. V. Tratnik and J. E. Sipe, Phys. Rev. A **38**, 2011 (1988).
[31] G. D. Peng, B. A. Malomed, and P. L. Chu, Phys. Scr. **58**, 149 (1998).
[32] G. Herring, P. G. Kevrekidis, B. A. Malomed, R. Carretero-González, and D. J. Frantzeskakis, Phys. Rev. E **76**, 066606 (2007); Lj. Hadžievski, G. Gligorić, A. Maluckov, and B. A. Malomed, Phys. Rev. A **82**, 033806 (2010).